Acta Acustica 2023, **7**, 26

https://doi.org/10.1051/aacus/2023021

Available online at:
https://acta-acustica.edpsciences.org

SCIENTIFIC ARTICLE OPEN ACCESS

Measurement of the diffuse field sound absorption using a sound field synthesis method

Samuel Dupont[1], Maryna Sanalatii[2], Manuel Melon[1,*], Olivier Robin[3], Alain Berry[3], and Jean-Christophe Le Roux[2]

[1] Laboratoire d'Acoustique de l'Université du Mans (LAUM), UMR 6613, Institut d'Acoustique – Graduate School (IA-GS), CNRS, 72000 Le Mans Université, France
[2] Centre de Transfert de Technologie du Mans (CTTM), 20 Rue de Thalès de Milet, 72000 Le Mans Cedex 09, France
[3] Centre de Recherche Acoustique – Signal – Humain (CRASH), Université de Sherbrooke, 2500 Bd de l'Université, Sherbrooke J1K 2R1, QC, Canada

Received 16 December 2022, Accepted 3 May 2023

Abstract – A method for measuring the diffuse field sound absorption coefficient of a material using sound field synthesis is proposed. A planar loudspeaker array is first used to generate acoustic plane waves with variable incidence angle on the surface of a material under test. Using a two-microphone probe positioned closely to the sample's surface, the angle-dependent sound absorption coefficients are then estimated. Finally, the diffuse field absorption coefficient is computed following Paris formula. Numerical simulations are used to evaluate the respective effects of the maximum incidence angle value and the number of individual incidence angles that are required for a robust calculation of the diffuse sound field absorption. Measurements are conducted on three different materials and compared with either simulation results obtained using the Johnson-Champoux-Allard theory, or with measurement results obtained using the standard reverberation chamber method. For all considered materials and over a wide frequency range, the proposed method leads to results that are in better agreement with theoretical predictions than those obtained using standardized methods.

Keywords: Sound field synthesis, Measurement method, Absorption coefficient, Diffuse field

1 Introduction

Sound absorbing materials are widely used in industrial sectors such as construction and transportation. Their performance is mainly characterized by the sound absorption coefficient. The values of this coefficient usually depend on the considered frequency and on the incidence angle of sound waves at the material surface. In practice, sound absorption values are usually averaged over the incidence angle (diffuse field measurement in a reverberation room), and over frequency (octave or third octave bands). Single-value ratings have also been proposed, such as the Noise Reduction Coefficient – NRC [1], the weighted alpha value or the sound absorption class [2].

The measurement of the diffuse field sound absorption coefficient by the reverberation room method has been standardized by the International Organization for Standardization [3] and the American Society for Testing and Materials [1]. This method is based on the use of the Sabine formula that requires the establishment of a diffuse acoustic field which is not always achieved in practice. Indeed, the results obtained using the reverberation room method suffer from well documented limitations such as a poor inter-laboratory reproducibility due to a large sensitivity to the sample's position, to microphones and sound source frequency response and position, lack of diffusors in the chamber, the presence of the tested material which modifies the acoustic intensity angular distribution, and edge diffraction effects [4–10]. All these effects result in large uncertainties in the measurement of the diffuse field sound absorption coefficient, with values that can exceed unity while the theoretical value shall be between zero and one. Although standards attempt to reduce the differences between laboratories by imposing a minimum room volume, minimum sample size, etc., each reverberation chamber deviates from the diffuse field assumptions in its own way, so the results obtained are not inherently reproducible. A future version of the ISO 354 standard is currently being drafted (Committee Draft stage) and proposes various solutions to improve the accuracy of the measurement method, such as the damping of the reverberation room, the use of a reference absorber, etc. However, the work of Scrosati *et al.* [9]

*Corresponding author: Manuel.Melon@univ-lemans.fr

has shown that although some of the proposals were beneficial, others could in some cases lead to increased variance between laboratories. The shortcomings of ISO 354 and ASTM C423-02 have these two important consequences: 1) the high variance between laboratory results does not allow comparisons of absorptive materials with confidence, 2) the overestimation of the absorption coefficient prevents the accurate prediction of reverberation times or sound pressure levels as reported in the literature [11, 12]. Indeed, the coefficients must be truncated or corrected to be used in building acoustics prediction software. This can lead to biased predictions, as well as additional iterations between simulation and field results to adjust the sizing of required soundproofing or sound control material (iterations that could be directly avoided with accurate data). This is particularly concerning, given that acoustic comfort has become increasingly important over the past decade, leading to the creation of several acoustical standards and regulations that have to be followed.

To overcome these issues, several approaches were proposed like *in situ* measurement methods under approximate diffuse field conditions. Takahashi *et al.* [13] used the background noise and a two-microphone probe placed in the vicinity of the material to measure the random incidence absorption coefficient in ordinary rooms. This technique was improved by using an ensemble averaging to calculate the normal surface impedance of a material under random excitation in a reverberation room to obtain its sound absorption coefficient [14].

Another approach is to use a microphone array and take advantage of this refined spatial information [15–19] to estimate the absorption coefficient for each incidence angle. Separation methods have also been proposed to split the incident and reflected energy flows and then calculate an angle-dependent absorption coefficient. For instance, double layer microphone array and Statistically Optimized Near-field Acoustical Holography (SONAH) [20, 21] have been used for *in situ* measurements while plane wave decomposition of pressure measurements performed in a small volume close to the tested material has been applied in a reverberation room [22] or in an ordinary room [23].

Further work has also been carried out to convert the values of the Sabine absorption coefficient, ideally intended to represent the absorption of an infinite slab of material excited by a perfectly diffuse sound field, into a random incidence absorption coefficient [24], accounting for non ideal conditions during the measurements. For this purpose, the effect of material size and the non-uniform distribution of the excitation field intensity are taken into account [25]. Good results have been obtained, but they depend on assumptions about the properties of the sample under test and cannot be generalized to all types of materials.

Another solution is to impose a target incident sound pressure field, typically using a loudspeaker array to radiate a target acoustic field. In practice, physical loudspeakers arrays are seldom used. A cost-effective and more efficient solution in terms of measurement resources is to use a virtual array in which a single loudspeaker is moved successively to different positions that loudspeakers would occupy in a physical array. Using measurements of transfer functions between each source and sensors placed in the vicinity of the material under test, it is possible to *a posteriori* generate target acoustic fields such as a plane wave at normal [26] or oblique incidence [27] or a diffuse field [28, 29] at a post-processing step, and calculate the corresponding sound absorption coefficients.

Using a Sound Field Synthesis (SFS) technique with a source array close to the material surface offers several benefits. Firstly, this ensures a large Signal-to-Noise Ratio. Secondly, this reduces the effect of the room reflections and edge diffraction by providing a strong direct signal. Finally, traditional microphone array methods deal with the problem as a consequence, while sound synthesis methods prevent the issues from occurring in the first place, providing a potential lever for removing room effects in the future.

This work falls into the SFS technique category, and more specifically by extending the results presented in Ref. [27] to calculate the diffuse field sound absorption coefficient of materials. This constitutes an alternative approach to the reverberation chamber method that would provide unbiased measurements between 100 Hz and 4 kHz by solving the classical issues resulting from the use of standardized approaches (ISO 354 or ASTM C423 methods). This paper also investigates the impact of angle step and maximum angle on the Paris formula, reports on the influence of sample size on the absorption coefficient results and compares the results obtained with the SFS method with those calculated with the JCA model or measured with the reverberation chamber method. The proposed approach leverages some of the limitations observed in the work published in Refs. [28, 29] for the estimation of the diffuse field sound absorption coefficient (maximum incidence angle limit, simplified spherical source-image model that leads to erroneous results at low frequency, *i.e.* when the product of the acoustic wavenumber and the source microphone distance is small). Furthermore, the theoretical framework proposed in this paper differs from that of Refs. [28, 29]: a plane wave formalism versus a spherical wave formalism, respectively.

It should be noted that one of the strengths of the proposed method is its relative simplicity, especially considering the complexity of the problem it addresses. The experimental setup requires only one sound source mounted on motorized stages and two microphones. The required calculations are based on a single measurement sequence and an integral calculation.

The paper is organized as follows: Section 2 recalls the principle of the method for measuring the oblique incidence absorption coefficient by sound field synthesis and extends it to the calculation of the diffuse field absorption. Numerical simulations using point sources are then performed in Section 3 to validate the method and to identify key parameters that influences the precision of the estimated results. Section 4 then presents experimental results that are compared with theoretical predictions and reverberation chamber measurements before summarizing the outcomes in Section 5.

2 Theory

2.1 Plane wave synthesis

Consider a planar, square, regular array of L loudspeakers, with $\sqrt{L} \in \mathbb{N}^+$, depicted in Figure 1 by dark bullets. The array's side length is denoted L_l, and therefore the source spacing is $\Delta_l = L_l/(\sqrt{L}-1)$. The array is placed parallel to and at a distance h from the surface of a material to be tested. This array is used to generate acoustic plane waves of arbitrary angle of incidence. To this end, the input signals of the loudspeakers are filtered out to reproduce target sound pressure fields on a square surface of side length L_m at the surface of the material ($z = 0$). The latter is sampled by M microphones, with $\sqrt{M} \in \mathbb{N}^+$, separated by $\Delta_m = L_m/(\sqrt{M}-1)$ (see white bullets in Fig. 1).

For each frequency f, the acoustic pressure $p_{lm}(f)$ generated by loudspeaker $l \in [1, L]$ at microphone $m \in [1, M]$ position is given by $p_{lm}(f) = g_{ml}(f)u_l(f)$, where $g_{ml}(f)$ is the source to microphone transfer function and u_l is its input signal. Note that in the simulations, a point source model is used for g_{ml} and $u_l(f)$ then corresponds to a source volume velocity whereas in the experiments $g_{ml}(f)$ is the measured transfer function and $u_l(f)$ is then the input voltage of loudspeaker l.

The vector of total sound pressure $\mathbf{p}$ at the M microphone positions due to the L loudspeakers can be calculated using a matrix formulation

$$\mathbf{p}(f) = \mathbf{G}(f)\mathbf{u}(f), \tag{1}$$

with $\mathbf{p} = [p_1(f), \ldots, p_m(f), \ldots, p_M(f)]^T$, $\mathbf{u} = [u_1(f), \ldots, u_l(f), \ldots, u_M(f)]^T$, where the superscript $^{\mathrm{T}}$ denotes the transposition, and

$$\mathbf{G} = \begin{bmatrix} g_{11}(f) & \cdots & g_{1l}(f) & \cdots & g_{1L}(f) \\ \vdots & \cdots & \vdots & \cdots & \vdots \\ g_{m1}(f) & \cdots & g_{ml}(f) & \cdots & g_{mL}(f) \\ \vdots & \cdots & \vdots & \cdots & \vdots \\ g_{M1}(f) & \cdots & g_{Ml}(f) & \cdots & g_{ML}(f) \end{bmatrix}. \tag{2}$$

The target sound pressure at the microphone positions, an acoustic plane wave $p_t(f)$ with prescribed incidence angles (θ, ϕ), is given by $\mathbf{p_t} = [p_{t_1}, \ldots, p_{t_m}, \ldots, p_{t_M}]^T$, with

$$p_{t_m} = e^{-jk(\sin\phi\cos\theta x_m + \sin\phi\sin\theta y_m)}, \tag{3}$$

where x_m and y_m are the coordinates of the mth microphone in the plane $z = 0$, $k = 2\pi f/c$ is the acoustic wave number and c the speed of sound in the air. The input signals of the loudspeakers are calculated by minimizing the error between the reproduced and target sound pressures as well as the squared inputs of the loudspeakers using the following cost function

$$\begin{aligned} \mathcal{L} &= (\mathbf{p}-\mathbf{p_t})^H(\mathbf{p}-\mathbf{p_t}) + \lambda\mathbf{u}^H\mathbf{u} \\ &= (\mathbf{G}\mathbf{u}-\mathbf{p_t})^H(\mathbf{G}\mathbf{u}-\mathbf{p_t}) + \lambda\mathbf{u}^H\mathbf{u}, \end{aligned} \tag{4}$$

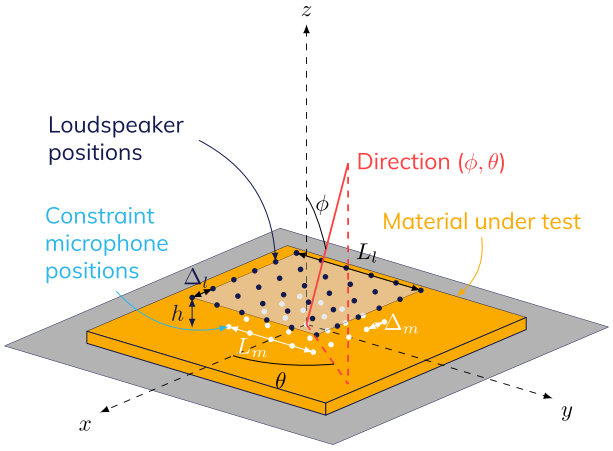

Figure 1. (Color online) Sketch of the measurement set-up. The dark blue bullets represent the locations of the loudspeaker while the white bullets represent the microphone positions for which the incident sound pressure field is constrained.

where the superscript $^{\mathrm{H}}$ denotes the Hermitian transpose and λ is a Lagrange multiplier. By differentiating equation (4), with respect to $\mathbf{u}$ and equating it to 0, the input signals u_t that minimize the above cost function at each frequency are given by

$$\mathbf{u_t} = \left[\mathbf{G}^{\mathbf{H}}\mathbf{G} + \lambda\mathbf{I}\right]^{-1}\mathbf{G}^{\mathbf{H}}\mathbf{p_t}. \tag{5}$$

2.2 Absorption measurement

The set-up described in Section 2.1 is used to synthetize an acoustic plane wave with prescribed incidence angles (θ, ϕ). The two-microphone technique [30] is then used to calculate the reflection coefficient under such excitation using the following expression

$$R(\phi) = \frac{H - e^{jkz_a\cos\phi}}{e^{-jkz_a\cos\phi} - H} e^{2jkd\cos\phi}, \tag{6}$$

where z_a is the elevation of the closest microphone with respect to the tested material, d is the microphone separation and $\mathrm{H} = p_{p1}/p_{p2}$ is the transfer function between the two microphones. Sound pressures p_{p1} and p_{p2} are respectively obtained at $(0, 0, z_a)$ and $(0, 0, z_2 = z_a + d)$. Note that the dependence on the plane wave azimuth angle θ does not appear in equation (6) as the tested sample is assumed to be homogeneous, isotropic and with large lateral dimensions. Thus, the estimated absorption coefficient only depends on ϕ, and is obtained as $\alpha(\phi) = 1 - |R(\phi)|^2$.

The calculation of the diffuse field absorption coefficient α_d from the angle dependant coefficient $\alpha(\phi)$ was first discussed in 1928 [31] thus proposing what became the so-called Paris law

$$\alpha_d = \int_0^{\pi/2} \alpha(\phi)\sin 2\phi \, \mathrm{d}\phi. \tag{7}$$

Improvements to this formula have been proposed to take into account the transition from a free field condition to an actual diffuse field [32, 33].

In this work, the Paris formula is used to estimate the diffuse field sound absorption coefficient, but with an upper integration bound. This limit is the maximum angle ϕ_{lim} above which the contribution of the absorption coefficient has a lower influence, because of the sin 2ϕ factor. Knowing the effect related to this maximum angle is interesting in practice as it is usually difficult to measure absorption coefficients for large incidence angles. The diffuse field sound absorption is then calculated as

$$\alpha_d = \frac{\int_0^{\phi_{\text{lim}}} \alpha(\phi) \sin 2\phi \ \mathrm{d}\phi}{\int_0^{\phi_{\text{lim}}} \sin 2\phi \ \mathrm{d}\phi}. \tag{8}$$

Note that the idea of using a higher integration bound has been used before, but rather to take into account the fact that ideally diffuse conditions cannot usually be obtained in real rooms, see for instance Ref. [34].

3 Numerical simulations

Numerical simulations are first reported to test the method under ideal conditions. A porous layer with a rigid frame is modelled using the Johnson-Champoux-Allard (JCA) model [35], see Appendix. Two different numerical evaluations of equation (8) are performed:

- The first one is used as a reference and labelled "Ref eval" in Figure 3. Equation (8) is computed with the analytical value of $\alpha(\phi)$ detailed in Appendix depending on the JCA parameters using the function *quad_vec* from the Python Scipy package [36] until a threshold error of 10^{-9} is reached.
- The second one, labelled "Dscrt eval", is performed by simulating the sound field reproduction process using equations (1)–(6) and performing the integration in equation (8) using the function *trapz* from the Python Numpy package [37]. It mimics the plane wave reproduction process and discrete measurements of $\alpha(\phi)$ over N_ϕ angles, as performed in experiments. The incidence angle is thus sampled over $[0, \phi_{\text{lim}}]$, with a discrete angular step $\Delta\phi_n = \phi_{\text{lim}}/(N_\phi - 1)$. An approximation of equation (8) is therefore obtained from this calculation.

Using these numerical evaluations, it is possible to study the influence of two key parameters on the estimation of α_d: (1) The discrete angular step $\Delta\phi$, and (2) the maximum incidence angle ϕ_{lim}.

The sound absorption coefficient of a 5 cm thick sample of polyurethane foam, PU1, is computed for various incidence angles using the "Ref eval" method. The JCA parameters for this material are given in column PU1 of Table 1. Results are shown in Figure 2 and highlight the angle dependence of the absorption coefficient of such absorbing materials.

In the proposed measurement procedure, the diffuse field absorption coefficient is calculated by averaging results obtained for discrete plane wave incidence angles (method "Dscrt eval"). Results obtained for equation (8) with $\phi_{\text{lim}} = 88°$ and for different discretization numbers $N_\phi = 3$, 6, 12 and 24 (and thus different angular steps $\Delta\phi = 44°$, 18°, 8° and 4°) are plotted in Figure 3. It can be noticed that the absorption coefficient reaches its analytical and reference value even for a limited number of discrete incidences N_ϕ: with 6 incidence angles the evaluation based on discrete angles almost perfectly coincides with the reference curve. To highlight this result, an error criterion is calculated: $\varepsilon_\alpha = |\alpha_{\text{ref}} - \alpha_{\text{Dscrt}}|$, where α_{ref} corresponds to the diffuse field absorption coefficient calculated with the "Ref eval" method while α_{Dscrt} is the one obtained with the discrete evaluation. In Figure 3, the error is less than 1% for $N_\phi \geq 6$. For a material exhibiting this type of angular dependence of the absorption coefficient, only a limited number of plane wave incidence angles (typically around 10) can be used to obtain a correct estimation of the diffuse field absorption coefficient.

Another significant parameter is the maximum incidence angle ϕ_{lim} in the computation of α_d. This parameter is particularly important because, as reported in the work of [27], the evaluation of $\alpha(\theta)$ by the proposed sound field synthesis becomes inaccurate for large incidence angles, typically above 60°. This is due to the difficulty in reproducing grazing plane waves with the source and microphone configurations depicted in Figure 1. Results computed with the "Ref eval" method are plotted in Figure 4 for various values of ϕ_{lim} between 45° and 88°. It is observed that for $\phi_{\text{lim}} \geq 78°$, the results are very close to the true absorption coefficient. Again, the error curves ε_α in Figure 4 provide a useful insight into the effect of the maximum angle of integration. A 78° value is consistent with the limit angle values reported in the scientific literature [13, 38] when using the Paris formula.

4 Measurements

4.1 Experimental set-up and method

The method described in Section 2 was tested experimentally. Measurements were performed in a semi-anechoic chamber using a single, moving loudspeaker instead of a full loudspeaker array. A FaitalPRO 3FE22 3″ loudspeaker, mounted in a closed box, with a bandwidth of 150–20 000 Hz at −3 dB, was moved over a regular square grid 50 cm above the tested porous layer using two Zaber linear motorized stages (Fig. 5). The value of 50 cm was chosen from the simulations carried out in Ref. [27], it allows the spherical pressure fields radiated by each of the sources to mix well enough to obtain a plane wave on the surface of the material under test. The source grid consists of 8×8 points forming a regular array of 1.05 m side length, resulting in a spacing between the sources of 15 cm and a Nyquist frequency of 1140 Hz. At the surface of the material, the incident acoustic field is constrained using equation (4) on a 20 cm square surface, regularly sampled

Table 1. JCA model parameters of the two polyurethane foams (PU1 and PU2) and glass wool (GW) used in numerical simulations and experiments.

Parameter	PU1	GW	PU2
Porous layer thickness h_p [m]	0.05	0.05	0.05
Flow resistivity σ [N s m^{-4}]	3320	13112	10605
Porosity ϕ [–]	0.97	0.954	0.956
Viscous characteristic length Λ [µm]	163	55.6	71.0
Thermal characteristic length Λ' [µm]	255	116	317
Tortuosity α_∞ [–]	1.06	1.0	1.67

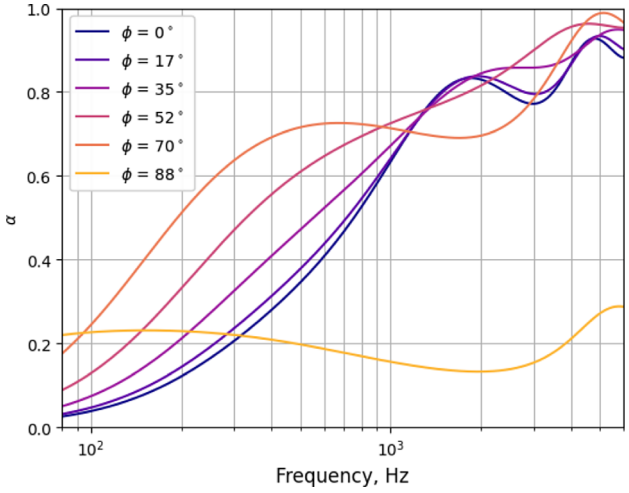

Figure 2. Theoretical absorption coefficient $\alpha(\phi)$ of material PU1 for various incidence angles. Values are computed using the "Ref eval" method.

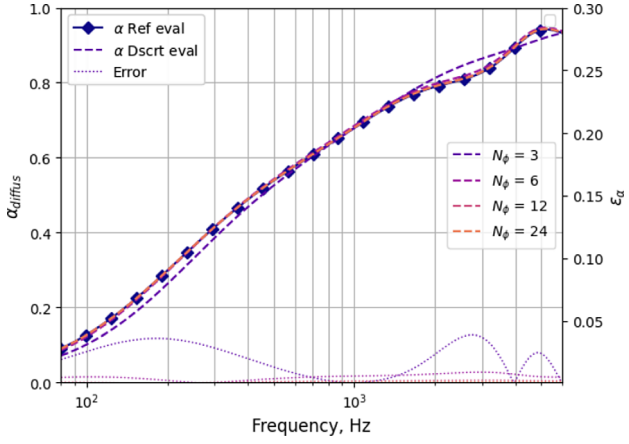

Figure 3. Absorption coefficient α_d and error criterion ε_α for material PU1 computed for different discretization numbers N_ϕ with $\phi_{\text{lim}} = 88°$.

by 13 × 13 virtual microphones, giving a sensor spacing Δ_m of about 1.7 cm. These geometric parameters have been optimized in [27] to provide an accurate estimation of $\alpha(\phi)$. The matrix $\mathbf{G}$ of source to constraint microphones in equation (1) was calculated assuming free-field conditions

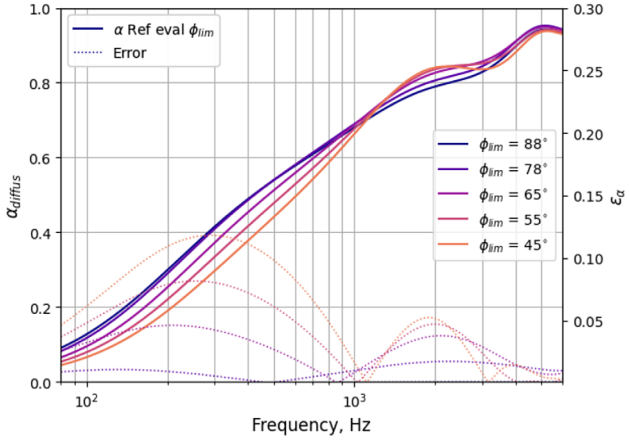

Figure 4. Absorption coefficient α_d and error criterion ε_α for material PU1 computed for various values of ϕ_{lim} using the "Ref eval" method.

and omnidirectional point sources. This assumption is further discussed in this section, and in [27].

A two-microphone probe with a $d = 3$ cm spacing was composed of two 1/4″ Brüel and Kjær microphones plugged to Nexus conditioning amplifiers. The lower microphone of the probe was set at $z_1 = 0.5$ cm from the material's surface. Generation of the loudspeaker signal for each source position and acquisition of the probe signals were performed via a custom Python code which controlled an RME Madiface XT audio interface. The excitation signal was a 12.1 s logarithmic sine swept signal ranging from 100 Hz to 7 kHz, amplified by a HPA D604 unit. Four averages per source position were performed to improve the signal-to-noise ratio and to obtain accurate transfer functions from each source position to each of the probe microphones. The measurement duration for 64 loudspeaker positions is approximately 2 h.

The measured transfer functions are then arranged in the following matrix $\mathbf{H_p}$:

$$\mathbf{H_p} = \begin{bmatrix} h_{11}(f) & \dots & h_{1l}(f) & \dots & h_{1L}(f) \\ h_{21}(f) & \cdots & h_{2l}(f) & \cdots & h_{2L}(f) \end{bmatrix}, \quad (9)$$

where h_{1l} and h_{2l} denote the transfer functions from loudspeaker l to microphone 1 and 2 respectively.

The following procedure is followed to calculate the absorption coefficient under any combination of angles ($\theta \in [0, 360°]$, $\phi \in [0, 90°]$):

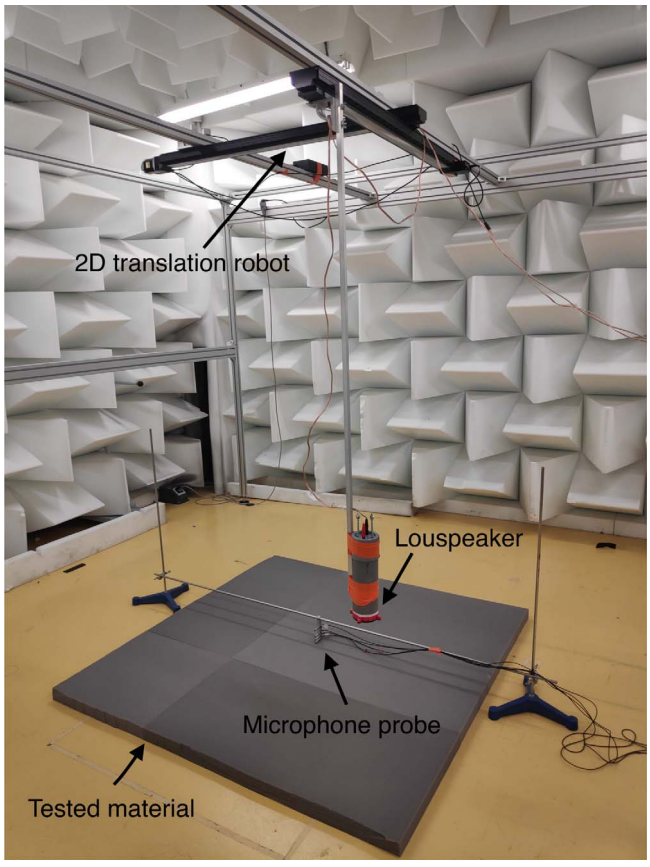

Figure 5. Experimental set-up installed in the Laboratoire d'Acoustique de l'université du Mans semi-anechoic room. The material under test is PU2, see Table 1.

1. Following a target sound pressure field, equation (3), the loudspeaker input signals u_t are calculated using equation (5) and the terms of the $\mathbf{G}$ matrix are calculated using a point source model. This assumption is satisfied up to approximately $ka = 1$, where $a = 3.2$ cm is the loudspeaker's radius, yielding an upper frequency limit of approximately 1700 Hz. A value of $\lambda = 10^{-7}$ is used unless otherwise stated.
2. The sound pressures at the microphone probe $\mathbf{p_b} = [p_{p1}(f), p_{p2}(f)]^T$, are calculated for each frequency using $\mathbf{p_b} = \mathbf{H_p}\,\mathbf{u_t}$.
3. $H(f) = p_{b1}(f)/p_{b2}(f)$ is finally calculated from $\mathbf{p_b}$ and used in equations (6)–(8) to obtain the sound absorption coefficients $\alpha(\phi)$ and α_d.

4.2 Experimental results

Nine square sections of 50 cm side length of polyurethane foam (PU1 material, see Tab. 1) were assembled to form a square of 1.5 m side length. The measured sound absorption coefficients for five values of ϕ are plotted in Figure 6. Note that the absorption coefficient $\alpha(\phi)$ was computed from the reflection coefficient $R(\phi)$ which has been linearly averaged over 10 values of the azimuth angle θ equispaced in [0°, 180°]. Averaging the reflection coefficient $R(\phi)$ along the azimuth angle assumes that the material has a behavior that does not depend on the angle θ. This assumption seems valid for the materials tested here, indeed polyurethane foams or glass wool generally exhibit an isotropic or transverse isotropic behavior. Moreover, the size of the tested materials combined with a near field excitation seems to be sufficient to limit the diffraction from the sample edges (this last point will be verified later on in Fig. 9). The standard deviation of the absorption coefficient (indicated by the shaded area of Fig. 6), is evaluated from the averages over azimuth angle.

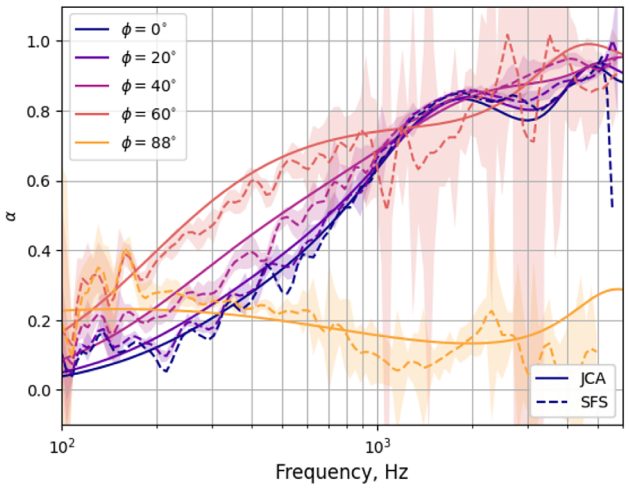

Figure 6. Theoretical (JCA) versus measured (SFS) plane wave absorption coefficient α of material PU1 for various plane wave incidence angles. The shaded zones indicate the standard deviation calculated from 10 linearly spaced values of azimuth angle θ.

The measured values and the absorption coefficient derived from the JCA model are in good agreement for incidence angles up to 60°. For $\phi = 60°$, the standard deviation calculated for 10 values of the azimuth angle θ is rather large. For $\phi = 88°$, the measured curve follows the theoretical prediction up to 3 kHz and then deviates from the expected results. In the low and medium frequency range, the oscillations observed in the absorption coefficient curves may be due to diffraction at the edges of the tested sample, as well as potential contributions from room modes. At high frequencies, the oscillations can be attributed to acoustic reflections from the motorized linear stages, and also to the mismatch between the hypothesis of an omnidirectional point source and the actual and more complex directivity of the used loudspeaker.

The values obtained for 15 ϕ angles ranging from 0° to 88° are averaged using the "Dscrt eval" method to evaluate the diffuse field absorption coefficient $\alpha_d(f)$ using equation (8). Results are shown in Figure 7 and compared to theoretical values calculated with "Ref eval" and the parameters of the JCA model given in Table 1. The two curves are in very good agreement from 100 Hz to 3 kHz. Theoretical and measured values in third octave bands are indicated with bullet points, showing also a very good agreement between

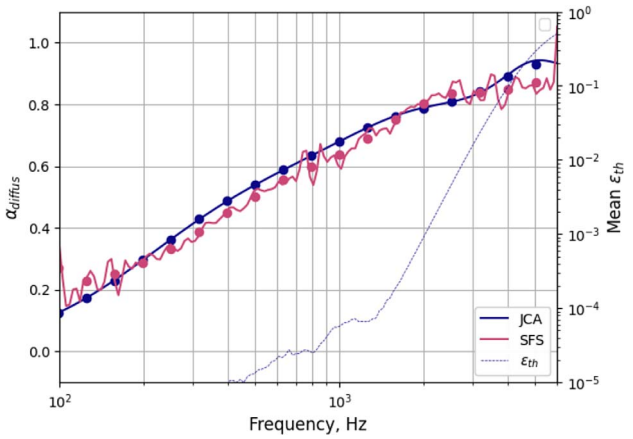

Figure 7. Theoretical (JCA) versus measured (SFS) diffuse field absorption coefficient α_d of material PU1 with $\phi_{\text{lim}} = 88°$ and $\lambda = 10^{-7}$. Averaged values for third octave bands are indicated by the round markers. The angle-averaged value of ε_{th} is also plotted.

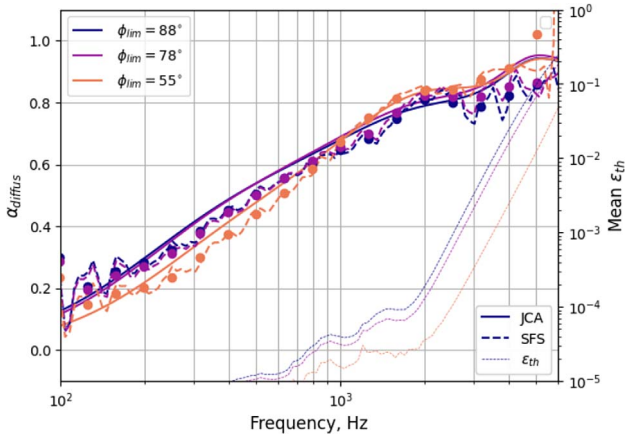

Figure 8. Theoretical (JCA) versus measured (SFS) diffuse field absorption coefficient α_d of material PU1 for different ϕ_{lim} with $\lambda = 10^{-7}$. The third octave band averages are indicated by the round markers. The angle-averaged value of ε_{th} is also plotted.

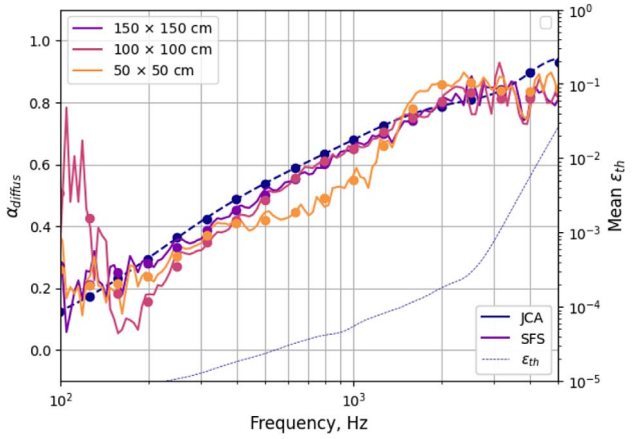

Figure 9. Theoretical (JCA) versus measured (SFS) diffuse field absorption coefficient α_d of material PU1 with $\phi_{\text{lim}} = 88°$ and $\lambda = 10^{-6}$. Measurements have been performed for three different material sizes. The third octave band averages are indicated by the round markers. The angle-averaged value of ε_{th} is also plotted.

experiments and theory. Figure 7 also shows the mean value of the reproduction error criterion ε_{th} given by

$$\varepsilon_{\text{th}} = \frac{|\mathbf{p_t} - \mathbf{G u_t}|_2}{|\mathbf{p_t}|_2}, \tag{10}$$

which estimates the deviation between the sound field $\mathbf{G u_t}$ radiated by the loudspeaker array assuming a point source model for the loudspeakers and the target plane wave $\mathbf{p_t}$. The ε_{th} curve in Figure 7 shows that the discrepancy between the experimental and theoretical absorption coefficients logically increases when the reproduction error ε_{th} becomes especially large (above 4000 Hz). In order to obtain accurate results at higher frequencies (and thus reduce ε_{th}), it is possible to reduce the distance between the source and constraint microphone arrays [27]. Reducing the size of the source array would, however, decrease the quality of the results at low frequencies. Further study should be carried out to optimize the bandwidth of the method for a given number L of sources. Another source of error at high frequencies is the directivity of the source used, that will not follow the omnidirectional assumption since the radius of the loudspeaker diaphragm becomes small compared to the acoustic wavelength (the loudspeaker enclosure also brings diffraction effects). This problem could be solved by measuring the actual directivity of the loudspeaker and incorporating it into the g_{ml} transfer functions.

As the accuracy of the proposed method decreases for large incidence angles, the effect of the maximum angle ϕ_{lim} considered in equation (8) is now investigated. The results given in Figure 8 show that a maximum angle of 55° is not sufficient to reconstruct a diffuse field absorption coefficient while results obtained with $\phi_{\text{lim}} = 78°$ and 88° are almost superimposed. This is expected since plane waves with large incidence angles provide larger absorption in low frequency (see Fig. 2). Nevertheless, the ε_{th} reproduction error curves in Figure 8 show that increasing ϕ_{lim} also increases the reproduction error since grazing plane waves are more difficult to reproduce with the experimental setup. As a consequence, the results obtained with $\phi_{\text{lim}} = 55°$ are closer to the theoretical diffuse field coefficient than the results obtained with larger values of ϕ_{lim} above 3 kHz.

Finally, the effect of the size of the tested material is studied using square samples with three side lengths: 50 cm, 100 cm and 150 cm. The matrix $\mathbf{H_p}$ is measured for each configuration, and used to compute corresponding α_d. Results are presented in Figure 9. The largest sample size provides the best agreement between theory and experiment, and over a wide frequency range. Absorption values obtained for the smallest side length largely deviate from the theoretical predictions, but the values obtained with a 1 m^2 area are very close to those obtained with the largest size (2.25 m^2 area) above 300 Hz.

Figure 10. Picture of the measurement set-up in the reverberation room showing the material under test, 5 of the 8 microphones and a group of two sources.

4.3 Comparison with reverberation chamber measurements

Comparison measurements were conducted in a reverberation chamber following a standardized procedure [3], see the picture in Figure 10. The volume of the reverberation chamber is 335 m^3, and reverberation times are measured using eight Bruël & Kjær 1/2″ microphones and two independent white noise signals generated simultaneously by two groups of two sources. Two materials are tested: a polyurethane foam (PU2) and a glass wool (GW), see Table 1 for their JCA parameters (the available surface for PU1 could not meet the requirement of ISO354 standard). A surface of 12 m^2 was used for the reverberation chamber measurements while an area of 1.5 m by 1.5 m was used for the sound field synthesis method. For the latter method, the following parameters were used: $\lambda = 10^{-7}$, $N_\phi = 15$, $N_\theta = 20$ and $\phi_{\text{lim}} = 88°$.

Results obtained for the PU2 material are plotted in Figure 11. Between 200 Hz and 2 kHz, the results obtained using the sound field synthesis method are in line the theoretical predictions, while results obtained using the standardized method show an overestimation of the absorption coefficient, with a maximum discrepancy of 0.18 at 400 Hz with theoretical predictions (33% overestimation). Above 2 kHz, the reproduction error increases rapidly and the sound field synthesis method leads to slightly underestimated sound absorption coefficient compared with theoretical predictions.

Note that the overestimation of absorption coefficients in the reverberation chamber is a known result. However, it seemed interesting to compare the results of the SFS method to both a theoretical model and to what is currently proposed by standards in order to illustrate the potential of the technique proposed here.

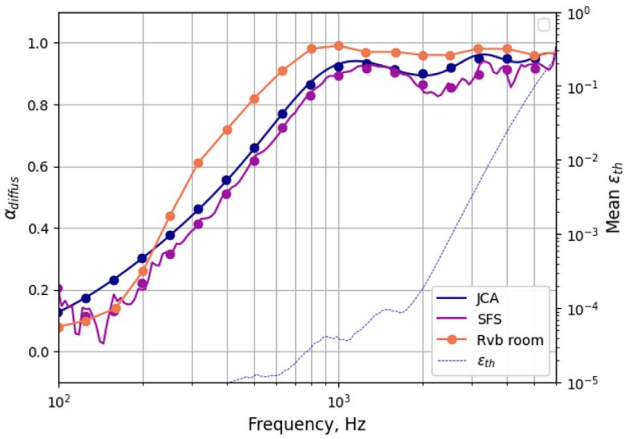

Figure 11. Comparison of the diffuse field absorption coefficient α_d of the PU2 material between JCA model predictions, reverberation room measurement and sound field synthesis method (with $\lambda = 10^{-7}$ and $\phi_{\text{lim}} = 88°$). The third octave band averages are indicated by the round markers. The angle-averaged value of ε_{th} is also plotted.

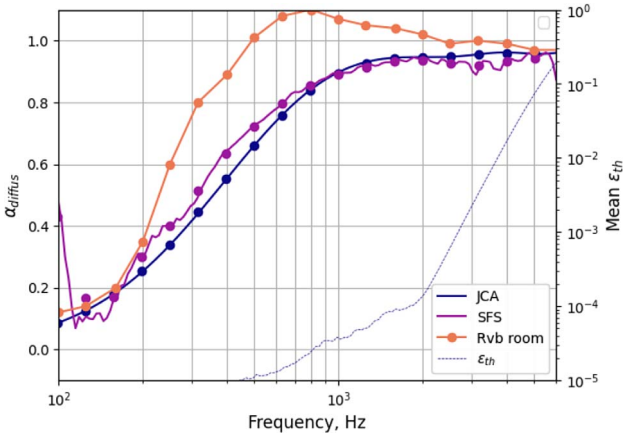

Figure 12. Comparison of the diffuse field absorption coefficient α_d of the GW material for three methods: JCA model, reverberation room and field synthesis method (with $\lambda = 10^{-7}$ and $\phi_{\text{lim}} = 88°$). The third octave band averages are indicated by the round markers. The angle-averaged value of ε_{th} is also plotted.

Results for the GW material are presented in Figure 12. The results obtained using the reverberation chamber method now largely overestimate the absorption coefficient values predicted using the JCA model. Values even exceed unity between 400 Hz and 2 kHz, with a maximum difference of 0.35 at 500 Hz (56% overestimation). The sound field synthesis results, like for the PU2 material, are in line with the theoretical prediction but with a slight overestimation of the absorption between 200 and 800 Hz (maximum difference of 0.08). This discrepancy is attributed to the

non-isotropic behavior of the glass wool, since an isotropic model was used to calculate theoretical values from parameters obtained under normal incidence.

5 Conclusion

In this paper, a sound field synthesis method was proposed and used to estimate the diffuse field sound absorption coefficient of materials. The method consists of generating plane waves with prescribed incidence angles and then measuring the corresponding absorption coefficient using a two-microphone probe. Instead of a physical loudspeaker array, a single and mobile loudspeaker is used and sound field synthesis calculations are performed at a post-processing step. The diffuse field absorption coefficient is then obtained by using a discrete version of the Paris formula. The method has been tested on three different materials and provided measured absorption coefficients close to values predicted with the JCA model between 150 Hz and 3 kHz. Compared with measurements conducted following the reverberation chamber method, the required sample area is reduced by a factor larger than 5, and the estimated sound absorption coefficients never exceed unity.

One direction for improvements is a bandwidth extension, in order to be able to characterize a material over octave bands from 63 Hz to 4 kHz. At low frequency, a loudspeaker with a lower cut-off frequency or a microphone probe with a larger spacing could improve the measurements. At high frequency, the use of coaxial loudspeakers and a properly tuned crossover filter could provide an omnidirectional source up to a higher frequency. Another solution is to measure the $\mathbf{G}$ matrix for all sources and constraint microphone positions as was done in [27], at the expense of a much longer measurement time. Another direction for improvements at large incidence angles could be to use a non-planar loudspeaker array, convex as an example. It is indeed more difficult for a planar array to radiate a plane wave in a direction with a large angle from the normal direction of the array.

Acknowledgments

This work was performed within the framework of the "Centre Acoustique Jacques Cartier", an International Research Project labeled by the Centre National de la Recherche Scientifique (CNRS). The authors would like to thank Nicolas Poulain at CTTM for performing the measurements used to obtain the parameters of the JCA model, James Blondeau and Félix Lebeuf for their help with the measurements.

References

1. ASTM C423:22: Standard test method for sound absorption and sound absorption coefficients by the reverberation room method. ASTM, West Conshohocken, PA, 2022, p. 2009.
2. ISO 11654:1997: Acoustics – sound absorbers for use in buildings – rating of sound absorption. International Organization for Standardization, Geneva, Switzerland. 1997.
3. ISO 354:2003: Acoustics – Measurement of sound absorption in a reverberation room. International Organization for Standardization, Geneva, Switzerland, 2003.
4. P.E. Sabine: The measurement of sound absorption coefficients. Journal of the Franklin Institute 207, 3 (1929) 341–368.
5. V.L. Chrisler: Dependence of sound absorption upon the area and distribution of the absorbent material. Journal of Research of National Bureau of Standards 13, 2 (1934) 169–187.
6. R.E. Halliwell: Inter-laboratory variability of sound absorption measurement. Journal of the Acoustical Society of America 73, 3 (1983) 880–886.
7. M. Vercammen: Improving the accuracy of sound absorption measurement according to ISO 354, in Proceedings of the International Symposium on Room Acoustics, Melbourne, Australia, 2010, pp. 1–4.
8. C.-H. Jeong, J.-H. Chang: Reproducibility of the random incidence absorption coefficient converted from the sabine absorption coefficient. Acta Acustica united with Acustica 101, 1 (2015) 99–112.
9. C. Scrosati, F. Martellotta, F. Pompoli, A. Schiavi, A. Prato, D. D'Orazio, M. Garai, N. Granzotto, A. Di Bella, F. Scamoni, M. Depalma, C. Marescotti, F. Serpilli, V. Lori, P. Nataletti, D. Annesi, A. Moschetto, R. Baruffa, G. De Napoli, F. D'Angelo, S. Di Filippo: Towards more reliable measurements of sound absorption coefficient in reverberation rooms: An inter-laboratory test. Applied Acoustics 165 (2020) 107298.
10. P. Didier, C. Van Hoorickx, E.P. Reynders: Numerical study of the accuracy and reproducibility of sound absorption measurements in reverberation rooms at low frequencies. Applied Acoustics 200 (2022) 109047.
11. M. Hodgson: Experimental evaluation of the accuracy of the Sabine and Eyring theories in the case of non-low surface absorption. Journal of the Acoustical Society of America 94, 2 (1993) 835–840.
12. S. Bistafa, J. Radley: Predicting reverberation times in a simulated classroom. Journal of the Acoustical Society of America 108, 4 (2000) 1721–1731.
13. Y. Takahashi, T. Otsuru, R. Tomiku: In situ measurements of surface impedance and absorption coefficients of porous materials using two microphones and ambient noise. Applied Acoustics 66, 7 (2005) 845–865.
14. T. Otsuru, R. Tomiku, N.B.C. Din, N. Okamoto, M. Murakami: Ensemble averaged surface normal impedance of material using an in-situ technique: Preliminary study using boundary element method. Journal of the Acoustical Society of America 125, 6 (2009) 3784–3791.
15. M. Tamura, J.-F. Allard, D. Lafarge: Spatial Fourier-transform method for measuring reflection coefficients at oblique incidence. II. Experimental results. Journal of the Acoustical Society of America 97, 4 (1995) 2255–2262.
16. J. Ducourneau, V. Planeau, J. Chatillon, A. Nejade: Measurement of sound absorption coefficients of flat surfaces in a workshop. Applied Acoustics 70, 5 (2009) 710–721.
17. J. Rathsam, B. Rafaely: Analysis of absorption in situ with a spherical microphone array. Applied Acoustics 89, 3 (2015) 273–280.
18. A. Richard, E. Fernandez-Grande, J. Brunskog, C.-H. Jeong: Estimation of surface impedance at oblique incidence based on sparse array processing. Journal of the Acoustical Society of America 141, 6 (2017) 4115–4125.
19. S. Dupont, M. Melon, A. Berry: Characterization of acoustic material at oblique incidence using a spherical microphone array. Journal of the Acoustical Society of America 147, 5 (2020) 3613–3625.

20. M. Ottink, J. Brunskog, C.-H. Jeong, E. Fernandez-Grande, P. Trojgaard, E. Tiana-Roig: In situ measurements of the oblique incidence sound absorption coefficient for finite sized absorbers. Journal of the Acoustical Society of America 139, 1 (2016) 41–52.
21. J. Hald, W. Song, K. Haddad, C.-H. Jeong, A. Richard: In-situ impedance and absorption coefficient measurements using a double-layer microphone array. Applied Acoustics 143 (2019) 74–83.
22. M. Nolan, S.A. Verburg, J. Brunskog, E. Fernandez-Grande: Experimental characterization of the sound field in a reverberation room. Journal of the Acoustical Society of America 145, 4 (2019) 2237–2246.
23. M. Nolan: Estimation of angle-dependent absorption coefficients from spatially distributed in situ measurements. Journal of the Acoustical Society of America 147, 2 (2020) EL119–EL124.
24. C.-H. Jeong: Converting Sabine absorption coefficients to random incidence absorption coefficients. Journal of the Acoustical Society of America 133, 6 (2013) 3951–3962.
25. C.-H. Jeong: Non-uniform sound intensity distributions when measuring absorption coefficients in reverberation chambers using a phased beam tracing. Journal of the Acoustical Society of America 127, 6 (2010) 3560–3568.
26. Y. Zhang, Z. Kuang, M. Wu, J. Yang: In-situ measurement of sound absorbing properties using plane-wave sound field reproduced by virtual loudspeaker array. Building and Environment 94 (2015) 883–890.
27. S. Dupont, M. Sanalatii, M. Melon, O. Robin, A. Berry, J.-C. Le Roux: Characterization of acoustic materials at arbitrary incidence angle using sound field synthesis. Acta Acustica 6 (2022) 61.
28. O. Robin, A. Berry, O. Doutres, N. Atalla, Measurement of the absorption coefficient of sound absorbing materials under a synthesized diffuse acoustic field. Journal of the Acoustical Society of America 136, 1 (2014) EL13–EL19.
29. O. Robin, A. Berry, C.K. Amédin, N. Atalla, O. Doutres, F. Sgard: Laboratory and in situ sound absorption measurement under a synthetized diffuse acoustic field. Building Acoustics 26, 4 (2019) 223–242.
30. J.F. Allard, B. Sieben: Measurements of acoustic impedance in a free field with two microphones and a spectrum analyzer. Journal of the Acoustical Society of America 77, 4 (1985) 1617–1618.
31. E. Paris: On the coefficient of sound-absorption measured by the reverberation method. The London, Edinburgh, and Dublin Philosophical Magazine and Journal of Science 5, 29 (1928) 489–497.
32. Y. Makita, T. Hidaka: Revision of the cos theta law of oblique incident sound energy and modification of the fundamental formulations in geometrical acoustics in accordance with the revised law. Acustica 63, 3 (1987) 163–173.
33. C.-H. Jeong: A correction of random incidence absorption coefficients for the angular distribution of acoustic energy under measurement conditions. Journal of the Acoustical Society of America 125, 4 (2009) 2064–2071.
34. M. Aretz, M. Vorländer: Efficient modelling of absorbing boundaries in room acoustic FE simulation. Acta Acustica united with Acustica 96, 6 (2010) 1042–1050.
35. J. Allard, N. Atalla: Propagation of sound in porous media: modelling sound absorbing materials 2e. John Wiley & Sons, 2009.
36. P. Virtanen, R. Gommers, T.E. Oliphant, M. Haberland, T. Blackdy, D. Cournapeau, E. Burovski, P. Peterson, W. Weckesser, J. Bright, S.J. van der Walt, M. Brett, J. Wilson, K.J. Millman, N. Mayorov, A.R.J. Nelson, E. Jones, R. Kern, E. Larson, C.J. Carey, I. Polat, Y. Feng, E.W. Moore, J. VanderPlas, D. Laxalde, J. Perktold, R. Cimrman, I. Henriksen, E.A. Quintero, C.R. Harris, A.M. Archibald, A. H. Ribeiro, F. Pedregosa, P. van Mulbregt, SciPy 1.0 Contributors: SciPy 1.0: Fundamental Algorithms for Scientific Computing in Python. Nature Methods 17 (2020) 261–272.
37. C.R. Harris, K.J. Millman, S.J. van der Walt, R. Gommers, P. Virtanen, D. Cournapeau, E. Wieser, J. Taylor, S. Berg, N.J. Smith, R. Kern, M. Picus, S. Hoyer, M.H. van Kerkwijk, M. Brett, A. Haldane, J.F. del Río, M. Wiebe, P. Peterson, P. Gérard-Marchant, K. Sheppard, T. Reddy, W. Weckesser, H. Abbasi, C. Gohlke, T.E. Oliphant: Array programming with NumPy. Nature 585, 7825 (2020) 357–362.
38. S.A. Yori: Method for calculating the sound absorption coefficient for a variable range of incidence angles. Archives of Acoustics 45, 1 (2020) 67–75.
39. J.-C. Le Roux, J.-P. Dalmont, N. Poulain: A new device for fluid equivalent parameters assessment, in Symposium on the Acoustics of Poro-Elastic Materials (SAPEM), March 29th–April 2nd, 2021, Purdue University, West Lafayette (Indiana), USA, 2021.
40. R. Panneton, X. Olny: Acoustical determination of the parameters governing viscous dissipation in porous media. Journal of the Acoustical Society of America 119, 4 (2006) 2027–2040.
41. X. Olny, R. Panneton; Acoustical determination of the parameters governing thermal dissipation in porous media. Journal of the Acoustical Society of America 123, 2 (2008) 814–824.

Appendix

A.1 Johnson-Champoux-Allard Model

The absorbing materials used in this paper are modelled using the equivalent fluid theory of Johnson - Champoux - Allard (JCA). The JCA parameters used to calculate the theoretical absorption curves are listed in Table 1. They were measured by taking circular samples from the tested materials and measuring their normal acoustic impedance in a tube equipped with an impedance sensor. The flow resistivity and the porosity are deduced from the low frequency behaviour of the normal impedance [39] while the other parameters are obtained by inverting an analytical model governing the wave propagation in the material [40, 41].

The absorption coefficient $\alpha(\phi)$ for any incidence angle ϕ is calculated using

$$\alpha(\phi) = 1 - \left| \frac{z_s(\phi) - \frac{z_0}{\cos(\phi)}}{z_s(\phi) - \frac{z_0}{\cos(\phi)}} \right|^2, \tag{11}$$

where z_0 is the characteristic impedance of air and z_s is the surface acoustic impedance of the material which is given by

$$z_s = -j \frac{z_p}{\cos \psi_p} \cot(h_p k_p \cos \psi_p), \tag{12}$$

where z_p is the characteristic impedance of the material and ψ_p is the angle of refraction in the material which is obtained from

$$\cos\psi_p = \sqrt{1 - \frac{k^2}{k_p^2}\sin^2\phi}. \tag{13}$$

The characteristic impedance of the porous medium is equal to

$$z_p = \sqrt{\rho_{\text{eff}} K_{\text{eff}}}, \tag{14}$$

while the complex wave number in the materials is given by

$$k_p = \omega\sqrt{\frac{\rho_{\text{eff}}}{K_{\text{eff}}}}. \tag{15}$$

The expressions of the effective density ρ_{eff} and bulk modulus K_{eff} of the porous medium depend on the material parameters listed in Table 1 and are given in [35].

Cite this article as: Dupont S. Sanalatii M. Melon M. Robin O. Berry A, et al. 2023. Measurement of the diffuse field sound absorption using a sound field synthesis method. Acta Acustica, **7**, 26.